Influence of different supply modes on the performance of linear induction motors

RYSZARD PAŁKA[1], KONRAD WORONOWICZ[1,2], JAN KOTWAS[1], WANG XING[3], HAO CHEN[3]

[1] *West Pomeranian University of Technology Szczecin*
al. Piastów 17,70-310 Szczecin, Poland
e-mail: ryszard.palka@zut.edu.pl, e-mail: j351994@gmail.com

[2] *Bombardier Transportation, Kingston, Ontario, Canada*
e-mail: konrad.woronowicz@rail.bombardier.com

[3] *China University of Mining and Technology, Xuzhou, China*
e-mail: wxstarwx@163.com, hchen@cumt.edu.cn

Abstract: This paper deals with the modelling of traction linear induction motors (LIMs) for public transportation. The magnetic end effect inherent to these motors causes an asymmetry of their phase impedances. Thus, if the LIM is supplied from the three-phase symmetrical voltage, its phase currents become asymmetric. This effect must be taken into consideration when simulating the LIMs' performance. Otherwise, when the motor phase currents are assumed to be symmetric in the simulation, the simulation results are in error. This paper investigates the LIM performance, considering the end-effect induced asymmetry of the phase currents, and presents a comparative study of the LIM performance characteristics in both the voltage and the current mode.

Key words: finite element analysis, linear induction motor, Péclet number, end-effect

1. Introduction

The linear induction motor based propulsion is a good choice for application in the aboveground, driver-less, short headway transit systems. The operations and maintenance data from the existing LIM-based urban transportation systems proves such systems to be much less expensive and vastly more reliable than the rotary-motor-based systems. The electromagnetic finite element analysis (FEA) calculations of the LIM performance are indirectly used to optimize the LIM based transportation system. The data obtained by the calculations is used for constructing the

force versus speed characteristics, which are subsequently utilized for the system performance computation [1, 2]. To minimize the LIM electromagnetic transient simulation time necessary to obtain a desired data point, the three-phase symmetrical currents are used in a constant current mode of operation [6, 7]. Otherwise, an external circuit would be necessary as part of the model, leading to an order of magnitude longer (or more) simulation time. Based on the method described in [10], this paper shows significant differences in slip versus thrust characteristics, obtained under the asymmetric current excitation, in both the voltage and the current modes of operation, of a LIM supplied from a standard 750 V dc traction inverter.

2. Problem formulation

Linear motors are commonly used in applications that range from the industrial material handling and low power amusement park drives to high power aircraft launchers and electric transit vehicles. Fig. 1 (left) shows an example of a LIM powered car of the Vancouver SkyTrain transit system and Fig. 1 (right) its in-ground installed LIM secondary, the so-called reaction rail (RR). To properly optimize the performance of a transit system, it is vital to predict or calculate the performance characteristics of a traction motor. This, in turn, allows for the prediction of energy flow and energy consumption and for an appropriate design of the ancillary systems such, for example, a traction motor cooling system. If the system's traction motor is an LIM, accounting for the asymmetry of phase currents becomes essential for the accuracy of the numerical performance analysis. This asymmetry must be properly derived from the physical phenomena or predicted indirectly by means of calculating the speed-dependent LIM phase impedances. This paper shows the results of LIM electromagnetic calculations including the effects of asymmetric excitation predicted by the latter method.

Fig. 1. SkyTrain car (left) and its reaction rail (right)

3. LIM finite element analysis

The following assumptions have been made about the structure of the LIM to simplify the calculation process:
1. Two-dimensional analysis can be used.
2. The iron magnetization curve is linear.

3. The conductivity of the reaction rail is constant.

4. The motion is in the x-direction.

In this case the electromagnetic field distribution within the LIM is described by the equation:

$$\frac{\partial^2 A}{\partial x^2} + \frac{\partial^2 A}{\partial y^2} = \mu \left(-J + j\omega\,\sigma A + \sigma\,v\frac{\partial A}{\partial x} \right),$$ (1)

wherein A is the z-component of the magnetic vector potential, J is the z-component of the current source density (z-component), ω is the angular frequency, v is the velocity in the x-direction and σ as well as μ are the conductivity and permeability, respectively.

The subject LIM is a six-pole, double-layer back wound motor with a pole pitch of 45 cm, 9-milimeter mechanical gap and 13.5 mm magnetic gap. The reaction rail is made of a 4.5 mm thick aluminum screen over an inch thick back iron.

Various analytical methods have been applied to calculate the electromechanical characteristics of the linear induction motors [1, 4]. Typically, such mathematical LIM models define the source currents as discrete coils or two dimensional continuous, sinusoidal current sheets [6]. The current sheet-based model is less realistic as compared to the discrete coils approach, as it neglects the spatial distribution of currents and in consequence the ensuing harmonics [7].

To determine all crucial parameters of a real LIM, the FEA should be applied rather than the analytical solution. One of the challenges which must be solved in the numerical FEA calculation is a proper evaluation of penetration of the electromagnetic field into the moving and conducting reaction rail. Such modelling and analysis can be extremely difficult and time-consuming as it requires a proper choice of the FE mesh, which depends on the velocity of the LIM and slip.

A characteristic (average) size h of finite elements in the conducting region of electrical machines (both: rotating and linear) is determined by the Péclet number [8, 9]:

$$P_e = \frac{\sigma\,\mu\,h\,|v|}{2}\,.$$ (2)

The skin-depth δ is the quantity which defines the penetration of an electromagnetic field into the conducting region:

$$\delta = \sqrt{\frac{2}{\omega\mu\sigma}}\,.$$ (3)

The Péclet number together with the skin-depth value give appropriate information about the magnetic field penetration into the conducting region and guide the evaluation of the FE mesh [10]. These adaptive requirements frequently lead to complex analytical equations and increase the potential instability of the numerical solutions.

4. LIM current versus voltage supply

The advanced LIM design must always take into account the so-called end-effect. The end-effect is caused by the demagnetization of the front of the motor due to currents induced in the reaction rail and strongly depends on the motor speed. Many aspects of the end-effect evaluation have already been analyzed in literature [10–13]. Fig. 2 shows the end part of the analyzed LIM.
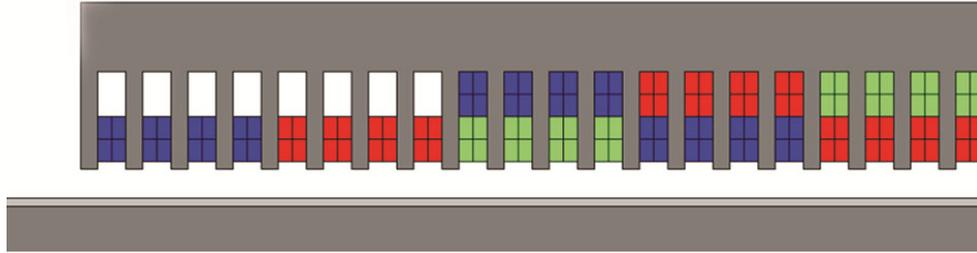
Fig. 2. End part of the LIM showing geometric assymetry and the asymmetric
phase windings distribution

Typically, the LIM is supplied from the voltage inverter converting thrust command into current by PWM control. However, as the impedances of the LIM are unequal, and the three-phase currents differ in their phase and magnitude, the negative sequence currents are produced leading to decreased motor performance. In theory, if the LIM phase impedances were known, the phase currents could be equalized, although not entirely, by a proper phase voltage control, but at a price of increased voltage harmonics. The electromagnetic fields shown below are calculated considering such unequal self- and mutual-inductances (impedances) of the LIM windings. Because the phase currents are magnetically coupled with one another and additionally coupled with the induced currents of the reaction rail, these impedances are frequency and speed dependent; thus, their determination can be very involving [10].

The next figure (Fig. 3) shows the magnetic field distribution within the subject LIM obtained by using COMSOL [14]. Infinite boundaries with zero magnetic vector potential were used for the left and right parts of the solution space and the zero magnetic vector potential at the top and bottom. As can be seen from the above picture the magnetic field shows a significant asymmetry on both ends of the machine. This causes an asymmetric back electromotive force coupling that leads to unequally coupled impedances and the asymmetry of phase currents.
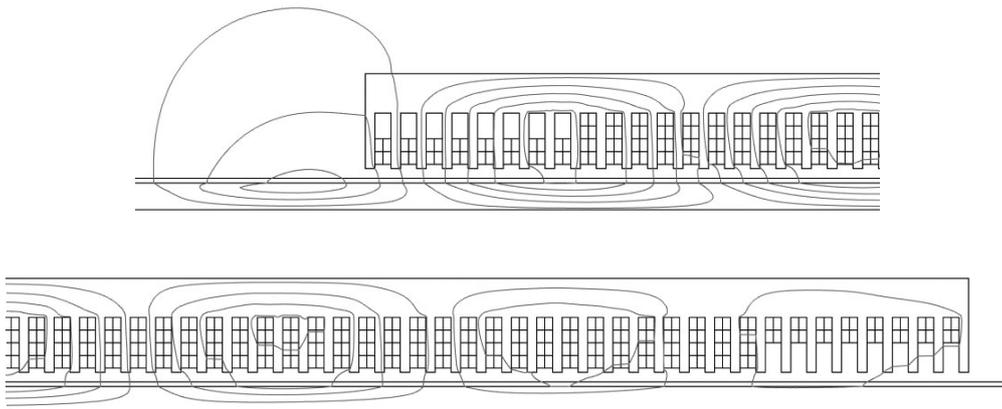

Fig. 3. Magnetic field distribution within the LIM

The next figure, Fig. 4, shows the results of longitudinal force evaluation for different supply modes. The curves described as "current_mode = 0" give results for the voltage supply and the curves described as "current_mode = 1" give results for the current supply.
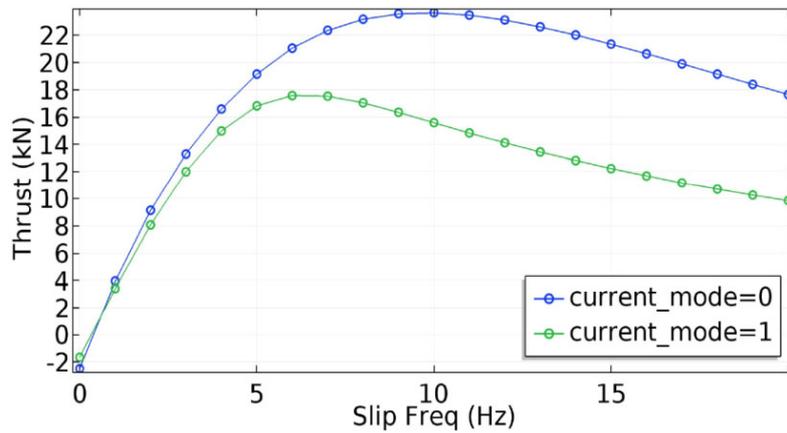

Fig. 4. Comparison of thrust values for both supply modes (v = 10 m/s, current mode: I = 550 A, voltage mode: V = 460 V)

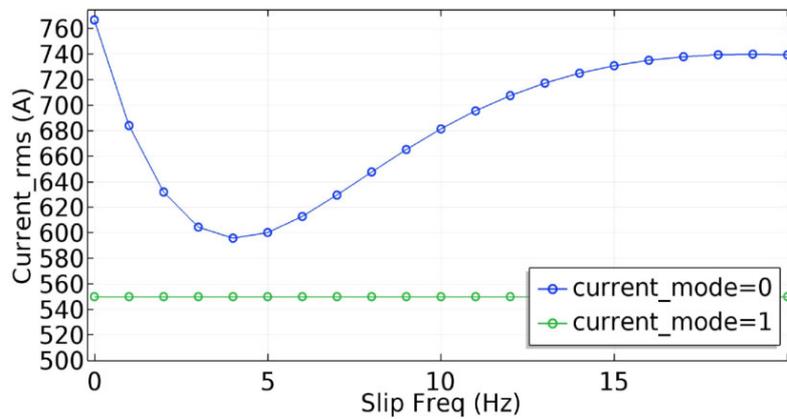The thrust dependencies from the above figure were obtained for the current values shown in Fig. 5.

Fig. 5. First phase current values for the voltage and current suppplies (v = 10 m/s)

As can be seen in Fig. 4 and Fig. 5, the thrust values for small slips are in both cases very similar but the current value for the voltage supply is much bigger. It is because the LIM impedance at that speed is still small and the phase current is higher than 550 A unless it is limited at that value by the inverter.

Fig. 6 shows total losses and primary losses for both supply modes. The losses in the voltage supply mode are much higher than in current supply.
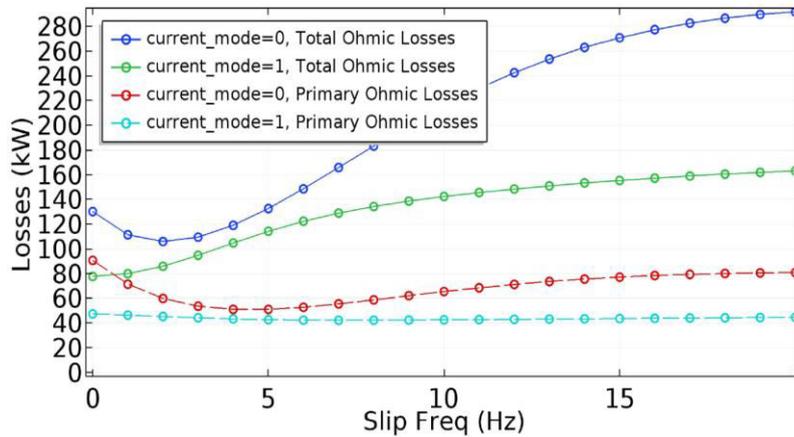

Fig. 6. Comparison of total losses and primary losses in the subject LIM for different supply modes ($v = 10$ m/s)

The next two figures illustrate the thrust values calculated for the subject LIM moving at 30 m/s, in both the voltage and the current mode. As can be seen, for the slip frequencies over 2 Hz, the motor current is limited by the impedance of the motor. Also, the peak performance (thrust) occurs at a much higher frequency than in the current mode and the rate of change of thrust around its peak is very low. In practice, it is always better to stay on the lower side of the peak thrust slip frequency to minimize the primary losses.
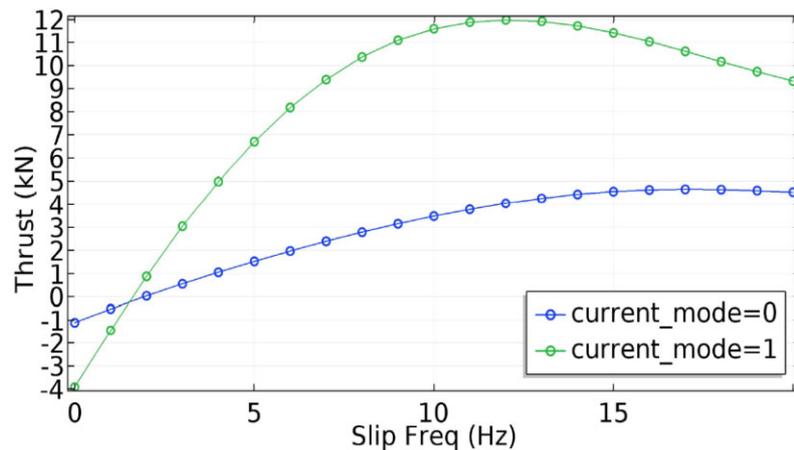

Fig. 7. Comparison of thrust values for both supply modes ($v = 30$ m/s, current mode: $I = 550$ A, voltage mode: $V = 460$ V)
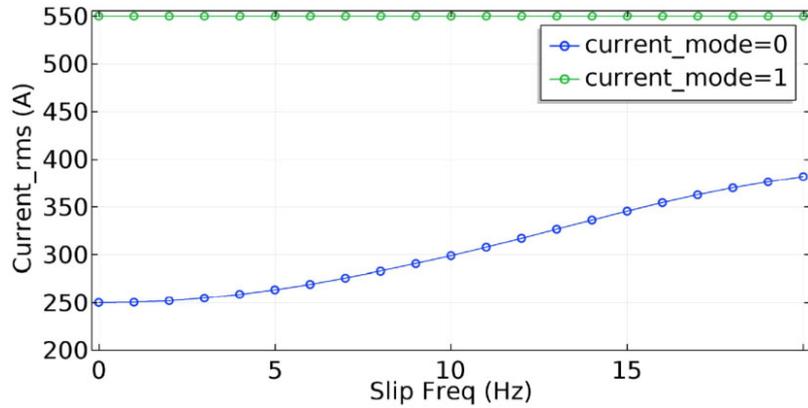
Fig. 8. First phase current values for the voltage and current suppplies (v = 30 m/s)

Total motor losses and primary losses for both supply modes of operation and for a speed of 30 m/s are given in Fig. 9. It shows that the losses in the voltage mode are lower when compared with the current mode. This is because at that motor speed the current is naturally limited in the voltage mode operation.
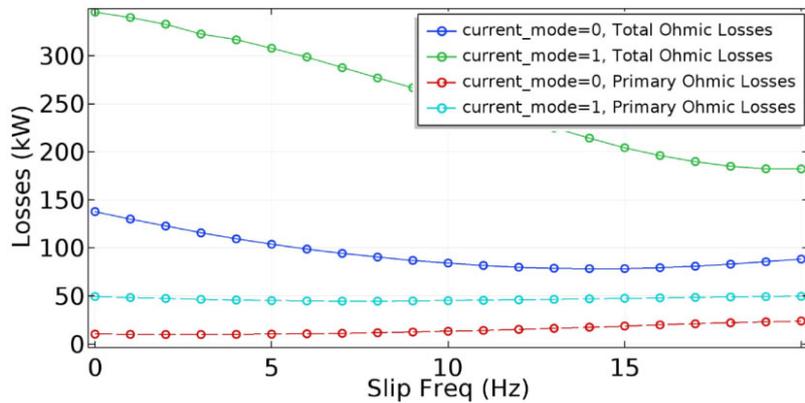

Fig. 9. Comparison of total losses and primary losses in the subject LIM for different supply modes (v = 30 m/s)

The performance characteristics of the subject LIM in current and voltage modes for different speeds are shown in Fig. 10 and Fig. 11, respectively. The characteristic increase of the peak performance slip frequency in speed results from the average end-effect induced magnetizing impedance change.

The following two figures (Fig. 12 and Fig. 13) show characteristics of the subject LIM for symmetrical and asymmetrical supplies, for selected speeds. The figures illustrate differences in the obtained thrust values.
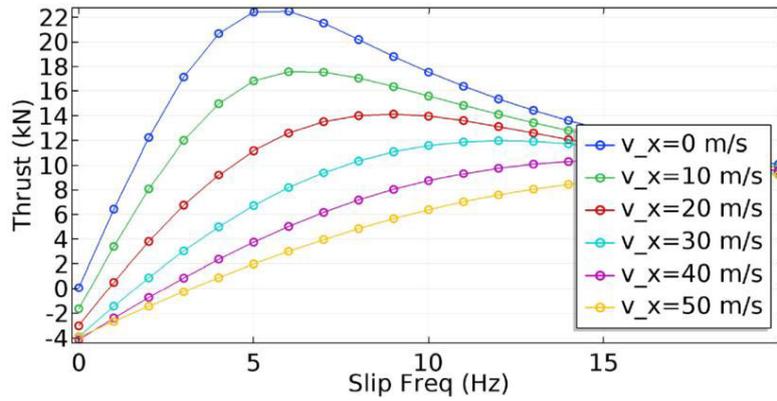
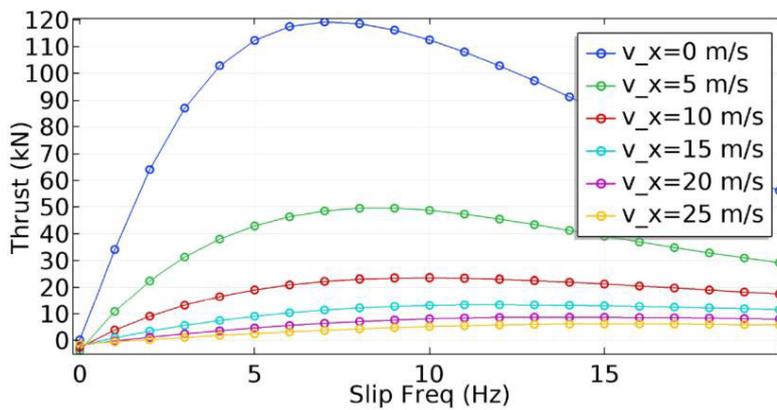Fig. 10. LIM characteristics obtained for the current-supply (I = 550 A)

Fig. 11. LIM characteristics obtained for the voltage-supply (V = 460 V)

Fig. 12. LIM characteristics obtained for the symmetrical (I = 550 A in all phases) and unsymmetrical supply (I_1 = 550 A, I_2 = 540 A, I_3 = 530 A) for the speed v = 10 m/s
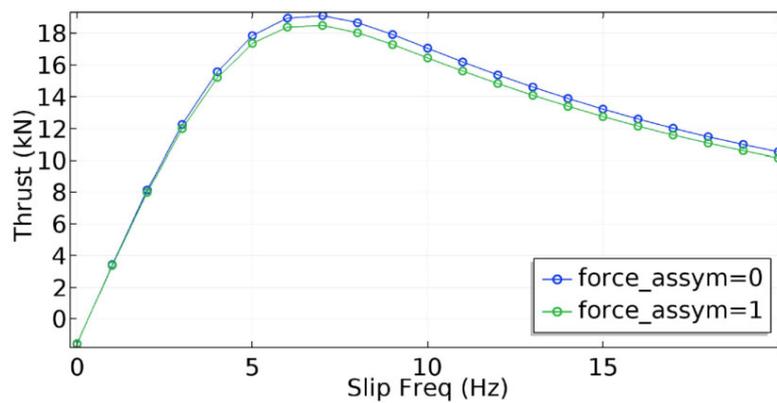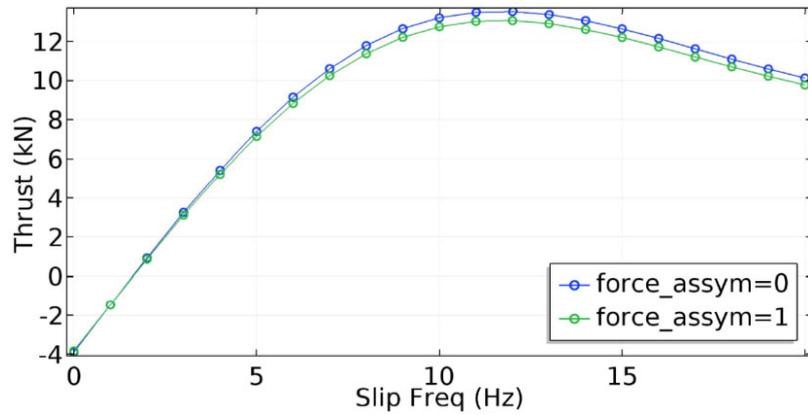
Fig. 13. LIM characteristics obtained for the symmetrical ($I = 550$ A in all phases)
and unsymmetrical supply ($I_1 = 550$ A, $I_2 = 540$ A, $I_3 = 530$ A) for the speed
$v = 30$ m/s

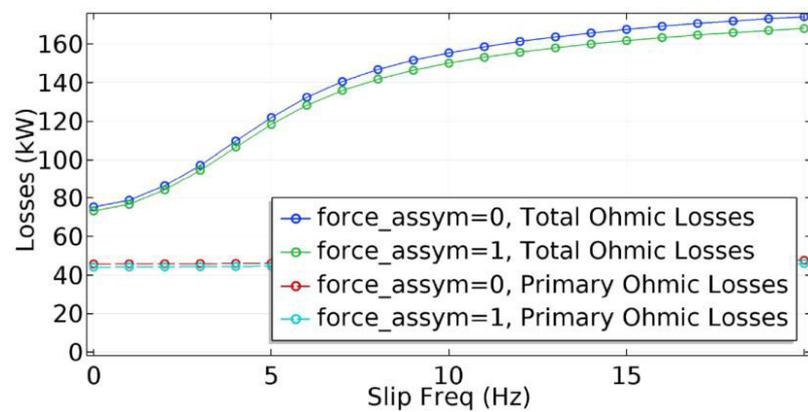Figs. 14 and 15 give the comparison of total and primary losses in the case of Figs. 12 and 13.

Fig. 14. Comparison of total losses and primary losses in the subject LIM for the
symmetrical and unsymmetrical supply ($v = 10$ m/s)

As can be seen from Figs. 12–15, it is important to account for the asymmetry of phase currents when trying to predict the LIM performance. In order to do that, the electromagnetic transient FEA simulation with the symmetrical three-phase voltage source must be used. However, this is prohibitively time consuming. Alternatively, the quasi steady state transient solution can be achieved simulating in frequency domain but only if the software allows for the modification of the Ampere's law like in COMSOL.
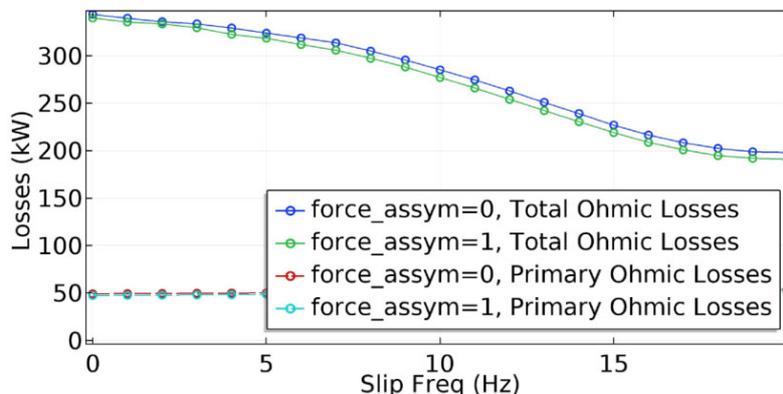
Fig. 15. Comparison of total losses and primary losses in the subject LIM for the
symmetrical and unsymmetrical supply (v = 30 m/s)

5. Conclusions

A set of performance characteristics of the LIM under symmetrical supply condition was presented for two selected speeds of a traction LIM. The analysis considers the end-effect induced impedance differences. It provides a very realistic performance prediction that can be used to properly control the slip frequency to minimize motor losses and to optimize the efficiency of the system. Future work will involve a way to replace the external circuit often used in electromagnetic transient simulations by introducing the state space equations of a LIM motor in an electromagnetic solver. This approach should generate the ultimate accuracy in determining the asymmetric current phasors and the resulting LIM performance. Subsequently, the work will include the effects of non-linear magnetizing characteristics and examine the saturation effects of both the primary and the reaction rail.

References

[1] Woronowicz K., Palka R., *An advanced linear induction motor control approach using the compensation of its parameters*, Electromagnetic Fields in Electrical Engineering, IOS Press, vol. 22, pp. 335–338 (2002).

[2] Woronowicz K., Palka R., *Optimised Thrust Control of Linear Induction Motors by a Compensation Approach*, International Journal of Applied Electromagnetics and Mechanics, vol. 19, pp. 533–536 (2004).

[3] Adamiak K., *A method of optimization of winding in linear induction motor*, Archiv für Elektrotechnik, vol. 69, pp. 83–91 (1986), DOI: 10.1007/bf01574843.

[4] Gieras J., Dawson G., Eastham A., *Performance calculation for single-sided linear induction motors with a double-layer reaction rail under constant current excitation*, IEEE Transactions on Magnetics, vol. 22, no. 1, pp. 54-62 (1986), DOI: 10.1109/TMAG.1986.1064270.

[5] Mendrela E.A., Gierczak E., *Two-dimensional analysis of linear induction motor using Fourier's series method*, Archiv für Elektrotechnik, vol. 65, no. 1–2, pp. 97–106 (1982).

[6] Abdelqader M., Morelli J., Palka R., Woronowicz K., *2-D quasi-static solution of a coil in relative motion to a conducting plate*, COMPEL – The International Journal for Computation and Mathematics in Electrical and Electronic Engineering, vol. 36, no. 4, pp. 980–990 (2017), DOI: 10.1108/COMPEL-07-2016-0312.

[7] Woronowicz K., Abdelqader M., Palka R., Morelli J., *2-D Quasi-Static Fourier Series Solution for a Linear Induction Motor*, COMPEL – The International Journal for Computation and Mathematics in Electrical and Electronic Engineering, vol. 37, no. 3, pp. 1099–1109 (2018), DOI: 10.1108/COMPEL-06-2017-0247.

[8] De Gersem H., Hameyer K., *Finite element simulation of a magnetic brake with a soft magnetic solid iron rotor*, COMPEL – The International Journal for Computation and Mathematics in Electrical and Electronic Engineering, vol. 21, no. 2, pp. 296–306 (2002), DOI: 10.1108/03321640210416386.

[9] De Gersem H., Vande Sande H., Hameyer K., *Motional magnetic finite element method applied to high speed rotating devices*, COMPEL – The International Journal for Computation and Mathematics in Electrical and Electronic Engineering, vol. 19, no. 2, pp. 446–451 (2000), DOI: 10.1108/03321640110383852.

[10] Palka R., Woronowicz K., Kotwas J., *Current Mode Performance of a Traction Linear Induction Motor Driven from the Voltage Converter*, Transportation Systems and Technology, vol. 4, no. 3, pp. 105–114 (2018), DOI: 10.17816/transsyst20184200-00.

[11] Abdollahi S.E., Mirzayee M., Mirsalim M., *Design and analysis of a double-sided linear induction motor for transportation*, IEEE Transactions on Magnetics, vol. 51, no. 7, pp. 1–7 (2015), DOI: 10.1109/TMAG.2015.2407856.

[12] Amiri E., Mendrela E.A., *A novel equivalent circuit model of linear induction motors considering static and dynamic end effects*, IEEE Transactions on Magnetics, vol. 50, no. 3, pp. 120–128 (2014), DOI: 10.1109/TMAG.2013.2285222.

[13] Woronowicz K., Safaee A., *A novel linear induction motor equivalent-circuit with optimized end effect model*, Canadian Journal of Electrical and Computer Engineering, vol. 37, no. 1, pp. 34–41 (2014), DOI:10.1109/CJECE.2014.2311958.

[14] Introduction to COMSOL Multiphysics, Version 5.3, © 1998–2017 COMSOL, available at: https://www.comsol.com/documentation.